TREAD RUBBER COMPOUND EFFECT IN WINTER TIRES: AN EXPERIMENTAL STUDY

Mohit Nitin Shenvi[*a], Adwait Verulkar [a], Corina Sandu[a], Hoda Mousavi[a]

[a] Terramechanics, Multibody, and Vehicle Systems (TMVS) Laboratory
Department of Mechanical Engineering, Virginia Tech, Blacksburg, VA 24060, United States
mshenvi@vt.edu, adwaitverulkar@vt.edu, csandu@vt.edu, hoda13@vt.edu

* Corresponding Author

This is the Author's Accepted Manuscript (AAM) of:

Shenvi, M. N., Verulkar, A., Sandu, C., and Mousavi, H. "Tread Rubber Compound Effect in Winter Tires: An Experimental Study." *Journal of Terramechanics*, Volume 99, February 2022, Pages 57-73, https://doi.org/10.1016/j.jterra.2021.11.004

Abstract

This paper presents an indoor experimental study focused on analyzing the effect of various tread rubber compounds on the tire performance on ice.

A set of sixteen tires (two per rubber compound) with identical dimensions, construction, and tread pattern, but of different tread rubber compounds, was investigated using the Terramechanics Rig which measures all forces and moments acting on a tire that is rolling (free or with slip) on ice. All operational parameters (normal load, inflation pressure, ice static coefficient of friction, ice temperature) were kept constant. Testing the tires under free rolling provided insights into the effect of the tread rubber compound on the resistive forces.

The investigation led to conclusive evidence that the tread rubber compound affects drawbar pull coefficient significantly (double for best than for the worst tire). It was found that the effect of the tread rubber compound in the lower slip region is most prominent, which is also where vehicles operate most of the time. The decrease in the stiffness is generally considered a positive sign for improvement in available friction but this cannot be a generalized conclusion when analyzing the tire as a whole, which is one of the major findings of this study.

Keywords: Tire-ice, winter tires, tread rubber compound, drawbar pull coefficient, resistive forces, genetic algorithm

Nomenclature

h(x)	Height of water film	[m]	η	Viscosity of water	[Pa.s]
ρ	Density of ice	[kg/m^3]	L	Latent heat of ice	[J/kg]
v	Velocity of sliding	[m/s]	λ	Thermal conductivity of ice	[Wm^{-1}K^{-1}]
T_m	Ice melting temperature	[°C]	T_{ice}	Ice bulk temperature	[°C]
C	Heat capacity of ice	[J/kg.K]	r_{eff}	Effective radius	[m]
r_L	Loaded radius	[m]	r_f	Unloaded radius	[m]

1. Introduction

The pneumatic tire is the part responsible for the creation or alteration of forces responsible for generating relative motion between a vehicle and the running surface. The running surface can generally be classified as rigid terrains (asphalt, ice, etc.) or deformable terrains (soil, snow, sand, etc.). Amongst the rigid terrains, icy roads are arguably the most challenging, due to the nature of available friction at the tire-ice interface. The friction available at the tire-ice interface is affected by the factors related to the tire as well as the ice.

It is common knowledge that of the total roadways in the United States, about 70% are in regions where the mean annual snowfall is more than 5 inches (US. Department of Transportation, 2020). The presence of ice or snow on top of the road also affects the handling of the vehicle and leads to a high number of accidents. Between 2007 and 2016, about 156,164 average annual crashes and 521 average fatalities were recorded every year due to accidents on icy pavements (US. Department of Transportation and Administration, 2020). These numbers provide a strong motivation to further study the tire-ice interaction. Since reducing the dependency of the safety of driving on the skills of the driver is also a concern, more attention to the improvement of the tire design and performance seems to be the logical conclusion.

This paper presents a part of a larger study related to the effect of tread rubber compound variation on the performance of the tire on ice. To fulfill the objective of the study, a set of sixteen tires (in subsets of two per rubber compound) were

investigated experimentally. These tires had identical design and construction, but different tread rubber compound. The tests were performed on an indoor test rig consisting of a single wheel tester, The Terramechanics Rig, at the Terramechanics, Multibody, and Vehicle Systems Laboratory (TMVS). In order to focus only on the effect of the tread rubber compound on the tire performance, all other parameters of operation were kept constant during testing. Prior works at the laboratory regarding testing on ice have had different goals like validation of the tire model used in the controller of an electric vehicle (Savitski et al., 2017) or comparison of the tire testing methodology if performed in an indoor lab (at TMVS) versus an outdoor field study (Bhoopalam et al., 2015a; Bhoopalam et al., 2015b).

This document is subdivided into the following sections. Section 2 consists of a detailed review of literature. Section 3 details the design of experiments. Section 4 includes the results from the experimental investigation and specific findings of this work. An attempt to parametrize the Magic Formula tire model using the Genetic Algorithm (GA) optimization technique led to insights about the effect of rubber compound, ambient temperature, etc. on the individual factors of the Magic Formula and is part of Section 5. Section 6 enlists the conclusions and directions for future work in this area of research.

2. Review of relevant literature

In this section, the results of the literature review related to the tire-ice contact phenomenon, the importance of the tread rubber compound in winter tires, and the effects of various tire parameters on the tire performance are presented.

2.1 Introduction to the tire-ice interaction

The high pressure at the tire-terrain contact is cited as one of the reasons for the inability of the classical laws of friction to describe the friction mechanism of tires (Moore, 1975). It is well known that the generation of friction at the tire-terrain interface can be attributed to adhesion and sliding. The adhesion component is more influential but faces a significant reduction when the terrain is contaminated with water or due to the presence of snow or ice (Blundell and Harty, 2004). In an experimental investigation focusing on the effects of surface roughness of rubber, two types of rubber samples having identical properties except for their surface roughness were tested under dry and lubricated friction conditions (Xu et al., 2013). In the case of the lubricated conditions, the friction of the textured rubber sample was detected to be higher in the low-speed region (<0.1 m/s). This trend, however, was reversed in the high-speed region, which was attributed to an occurrence of micro-cavitation effect and an amplification in the formation of the water film. The results of these tests followed the trend expected by the Stribeck curve.

Having an icy surface for the terrain further increases the complexity of the analysis of the friction mechanism. A quasi-liquid layer of melted ice, having a low shear strength near the melting point, is generally held responsible for this effect (Nakajima, 2019). The temperature of the ice near to the melting point will further increase this complexity as the melt-freeze cycle is dominant leading to higher number of accidents. An increase in the velocity of the rubber block or normal load would increase the heat generated due to friction leading to an increase in the height of the water film present at the tire-ice contact. Hence, the normal load on the tire, the velocity of the tire against the ice (sliding velocity), and the temperature of the ice are crucial and dominate the friction mechanism in the contact patch of tire-ice interaction. A study (Sokolovskij, 2007) of the braking and traction characteristics on different road surfaces led to a range of traction coefficients; the ones relevant to ice are presented in Table 1.

Table 1
Range of the coefficient of traction on ice. Adapted from (Sokolovskij, 2007)

Ice Surface Type	Description of surface	Traction Coefficient, Φ
Smooth Ice	Sufficiently thick layer of ice without any traces due to studs, chains, etc.	0.054-0.19
Black Ice	Thick ice layer appearing like a black wet road, not easily distinguishable by the driver	0.12-0.26
Ice (with chains mounted on tires)	A layer of ice (sufficiently thick) with traces due to the movement of wheels having steel chains	0.12-0.18

2.2 Importance of the tread rubber compound in winter tire performance

The drawbacks of other tires during cold or icy conditions gave a great boost to the development of winter tires that were introduced initially in the studded variant. The studded tires had small pins in the tread, which were useful to cut into the ice surface in order to reduce slipping and improve the grip of the tire on the ice. The main drawback of these tires was that in the non-winter conditions, the pins could cause damage to the asphalt pavement and also lead to the noise issue. Due to these reasons, the use of these types of tires is now prohibited in many countries.

To overcome these drawbacks and with the improvements in the technologies of rubber compounding and tire siping, studless winter tires received a boost. A higher number of sipes, specific design of the tread pattern, higher tread depth, and the rubber compound used are the pertinent features of these tires which concentrate on the removal of the melted water film, reduction of the buildup of snow, increase in the real area of contact, etc. for improved performance. From the working of the tire, the tread is the main part of the tire that is in contact with the ice. So, the tread rubber and its properties are responsible

for dictating the performance a tire has on ice and, thus, it is a reason for renewed interest in the research of the field. In winter tires, the rubber compound of the tread is generally softer to account for the change in its stiffness due to the cold conditions faced by it which is responsible for the reduction of the grip. Siping technology, though an important parameter, was found to be limited in its role in improving the friction by (Ripka et al., 2012). It was found that the sipes per tread block could increase the friction only up to a limit and reduce it after that, as shown in Figure 1. Thus, the study of the tread rubber compound seems to be the logical way forward for improvements in winter tires.

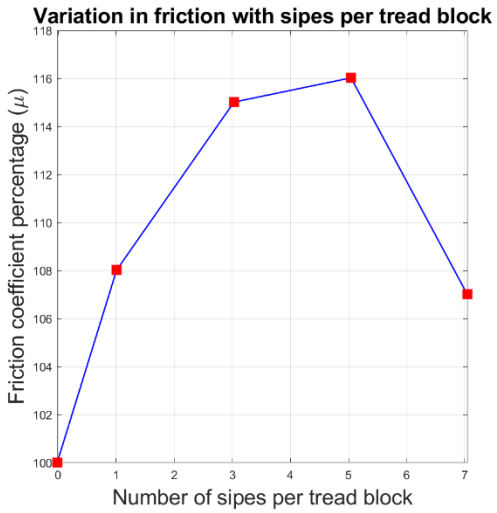

Figure 1: Variation in the coefficient of friction with a change in the number of sipes. Redrawn in agreement to the plot in (Ripka et al., 2012)

2.3 Effects of rubber compound on the rubber-ice friction

The various studies focusing on the effect of the rubber properties on the friction between rubber and ice need to be understood in order to have a better point of view while approaching the effect of tread rubber compound on the tire-ice friction. A comparison of the theoretical formulations and indoor experiments for rubber-road contact is presented in (Motamedi et al., 2016). In a study (Persson, 2006), the importance of the role of flash temperature in the rubber-asphalt friction was investigated. It was found that the flash temperature dictates the friction mechanism when the velocities are more than 0.01 m/s. This effect would be more prominent when we consider the terrain to be ice, especially near its melting temperatures, as this flash-temperature effect would increase the amount of water film in the contact patch due to the melting of ice in this region. It was also found that the change in the shape of the contact patch (keeping the normal load and contact pressure constant) does not affect the friction-slip curve much (Persson, 2011), as shown in Figure 2. The author also found

that with an increase in the contact pressure, the friction of rubber decreased as shown in Figure 3. The inflation pressure and normal load were consistent during the testing of all tires in this work.

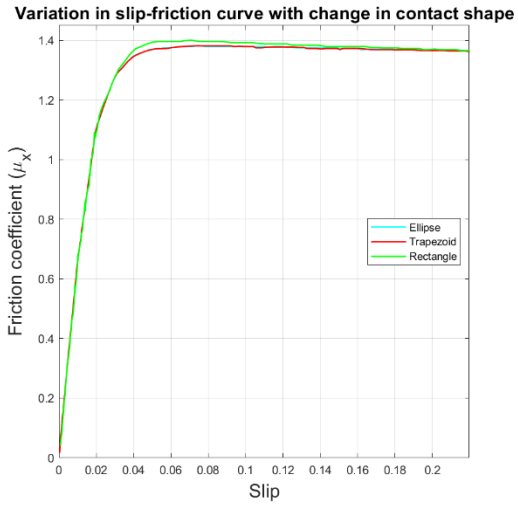

Figure 2: Effect of change in contact shape on the friction with a change in slip ratio. Redrawn in agreement to the plot in (Persson, 2011)

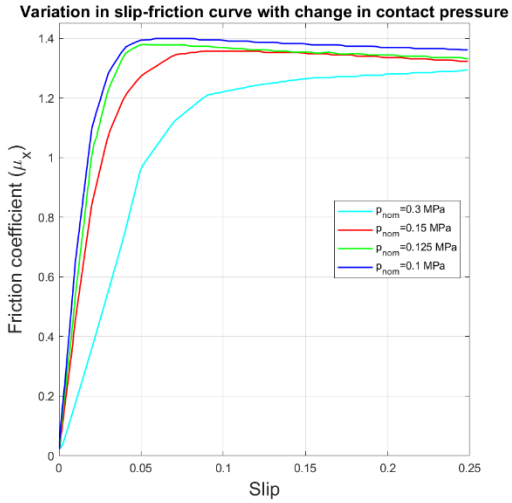

Figure 3: Effect of change in contact pressure on the friction with a change in slip ratio. Redrawn in agreement to the plot in (Persson, 2011)

In another work (Persson, 2014), the role of frictional heating was analyzed and derived using a non-uniform motion theory and it has been concluded that a part of the frictional energy is produced due to interlayer friction within the rubber itself. The role that the rubber physical and mechanical properties can play in the friction between rubber and ice were

validated as if this effect was considered; the inter-layer friction changes depending on the composition of the layers and the nature of the dispersion of elements within the rubber.

Authors of the work (Skouvaklis et al., 2012) investigated rubber-ice friction experimentally testing three different rubber compounds at different normal loads and temperatures. The velocity of the rubber sample ranged between 0.1 m/s and 1 m/s. The effect of change in the source of water used (tap water or de-ionized water) in creating ice, on the friction, was explored, too. An increase in the temperature and sliding velocity was found to have a detrimental effect on the friction coefficient. The reduction in friction coefficient at high temperatures and velocities was attributed to the melting of ice and subsequent presence of water layer however the friction mechanism was found to be dominated by the viscoelastic properties of rubber at lower speeds. It was found that the softer rubber exhibited a higher friction coefficient as shown in Figure 4, and this is postulated to be the effect of an increase in the real area of contact.

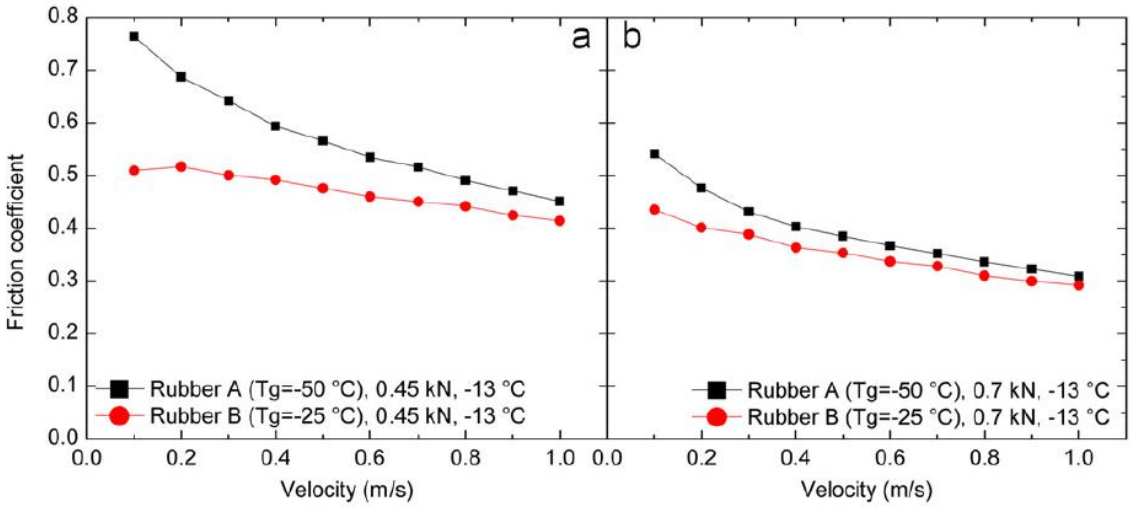

Figure 4: Comparison of the coefficient of friction for two rubbers with different properties (Skouvaklis et al., 2012). Reprinted with permission from Elsevier

In the analytical modeling approach developed (Wiese et al., 2012), the evaluation of the height of water film is performed using a derivative of length representation (as in eq. (2)) instead of a derivative of time representation (as in eq. (1)), based on the Greenwood-Williamson contact theory (Greenwood and Williamson, 1966). The eq. (2), shows the effect on the height of water film formed at the rubber-ice contact due to the parameter of roughness, 'k_x', and consequently on the friction coefficient. The results of this modeling approach are validated by comparing them with the experimental results obtained by the authors.

$$\frac{dh(t)}{dt} = \frac{\eta}{\rho L}\frac{v^2}{h(t)} - \sqrt{\frac{\lambda C}{\pi \rho L^2}}\left(\frac{T_m - T_{ice}}{t^{\frac{1}{2}}}\right) \quad (1)$$

$$\frac{dh(x)}{dx} = \frac{\eta}{\rho L}\kappa_x\frac{v^2}{h(x)} - \sqrt{\frac{\lambda C}{\pi \rho L^2}}\left(\frac{T_m - T_{ice}}{(v.x)^{\frac{1}{2}}}\right) \quad (2)$$

A work (Klapproth et al., 2016) focusing on the development of a viscous model for analyzing the friction between the rubber and ice, postulated that if there is no transient behavior, the percentage of hysteretic friction will be negligible. In this work, the influence of several parameters like the stiffness of the rubber, sliding velocity, temperature of ice, nominal pressure, etc. were investigated and the effect on the rubber-ice friction due to variation in the stiffness of the rubber compound was modeled qualitatively. It was also concluded that, though the softer rubber compound has higher friction, at high nominal pressures (5 bar in the study) the harder rubber compound has the higher friction coefficient as shown in Figure 5, which is attributed to the saturation effect.

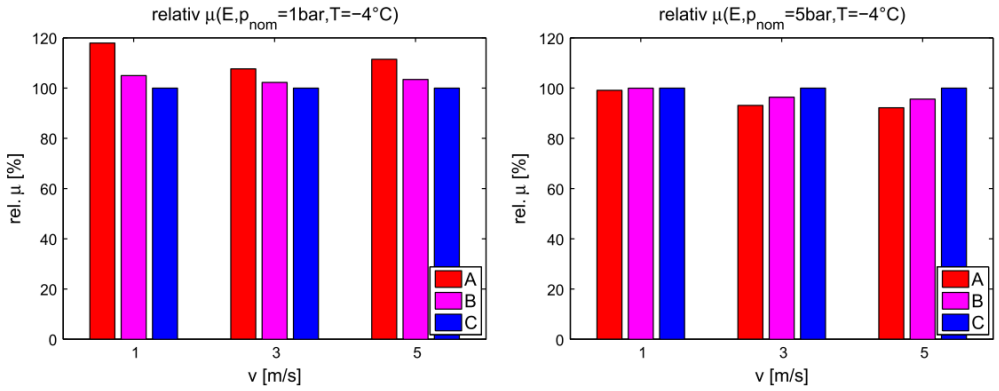

Figure 5: Ranking of percentage friction coefficient for 3 rubber compounds at 1 bar and 5 bar nominal pressures respectively (Klapproth et al., 2016). Reprinted with permission of Elsevier.

A tribological study (Isitman et al., 2017) about the performance of rubber on ice due to the stiffness of the rubber and surface roughness of rubber led to a major conclusion that the dynamic friction coefficient is in inverse proportion to the stiffness of the rubber. The examination of the influence of the filler material was attempted and could be a foundation to further analyze its effects on the performance of the tire.

Rubber ratio, a term representing the ratio between the actual contact area and apparent contact area, was defined and analyzed while analyzing the tire-ice interaction (Zhang et al., 2018). They concluded that the optimal range for the rubber

ratio to improve the friction on ice would be 0.64-0.76. An in-depth analysis of this study could also include the effects of the tread pattern, assuming a constant rubber ratio.

The influence of siping edges on the coefficient of friction in the tire-ice interaction was the focus of (Yamazaki et al., 2000). The authors determined that the effect of sipes is negligible if the velocity is very low or the temperature is nearing the melting point. As both of these conditions were fulfilled and constant during our work, in addition to the tires being identical in design, this effect was neglected in this work.

In a finite element analysis of a winter tire on ice conducted by (Jung et al., 2018) it was determined that the compounds of the undertread of a tire do not affect its performance much when comparing with the effect that the compounds of the tread has on the performance of the tire. The friction coefficient was found to be reduced as the temperature of ice neared 0°C as well as with an increase in the sliding velocity, as depicted in Figure 6.

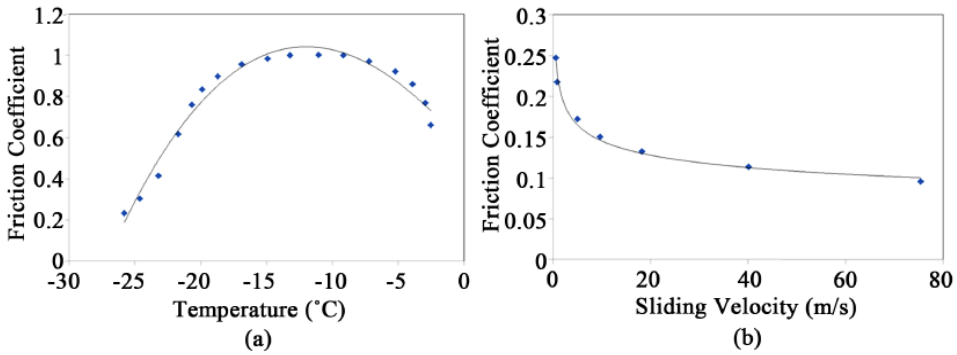

Figure 6: Effect of change in temperature and sliding velocity on the friction coefficient of winter tire on ice (Jung et al., 2018). Reprinted under Creative Commons License (CC BY 4.0)

2.4 Effects of variation in ambient temperature on the tire performance on ice

An examination of the friction phenomena between rubber and icy asphalt pavements was performed (Tan et al., 2020). The authors found that there is a significant effect on the friction coefficient in icy surfaces due to variation in the ambient temperature. The ambient temperatures used for the testing were -5°C, -10°C, and -20°C. It was concluded that an increase in the ambient temperature would lead to a decrease in the coefficient of friction. It should be noted that the considered ambient temperatures during this work were negative, which is more realistic of cold regions with icy conditions in the majority of the cases.

Another investigation (Bhoopalam et al., 2015a) studied the impact of change in ambient temperature on the performance of the tire on ice. The drawbar pull coefficient was found to decrease with a reduction in the ambient temperature when the ambient temperatures considered were positive, as shown in Figure 7. The reasons for this could be two-fold. First, the material properties of the rubber would get affected due to a reduction in the surrounding temperature. Secondly, when the ambient temperature rises in the positive domain, it will have an effect on the properties of ice, especially on the surface.

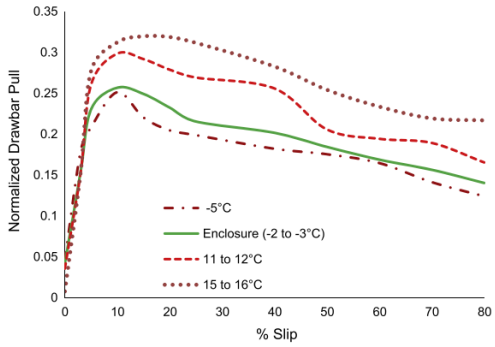

Figure 7: Effect of variation in ambient temperature on the drawbar performance of the tire on ice with all the parameters constant (Bhoopalam et al., 2015a). Reprinted with permission from Elsevier.

Thus, in the experimental setup at TMVS laboratory, the authors attempted to nullify the effect of ambient temperature during testing by conducting the tests when the ambient temperature was nearly constant.

3. Experimental Approach and the Design of Experiments

The Terramechanics rig at TMVS lab was designed (Sandu et al., 2008) with the testing of a single wheel on various terrains being the primary goal. Variations in the operational parameters like the normal load on the tire, the inflation pressure of the tire, slip ratio, toe angle, camber angle, etc. are possible. The rig has had several improvements over the years, with the most recent modification being the introduction of a clutch and brake assembly done in order to test the free-rolling and braking conditions on a tire (Khan and Sandu, 2017). The clutch mechanism is installed between the wheel motor (one of the two motors of the rig) and the wheel hub. The wheel motor is used to provide torque in order to simulate a specific slip ratio condition and the clutch is disengaged for testing the free-rolling condition. The carriage motor provides linear movement to the carriage and in turn to the wheel at a constant rate of 0.06 m/s. This is also the velocity considered while calculating the velocity at a certain slip condition. The application of slip ratios is done using the PicPro software while the Active Normal Load Controller system (Naranjo, 2013) is controlled using the NI Labview software which controls a proportional valve. A

change of about 0.05 V creates about 75 N variations in the normal load. The normal load value through this method though was found to be in a close range of the targeted normal load instead of a constant normal load value (Mousavi et al., 2019).

The Kistler P650 hub, which is a part of the Terramechanics rig is a sensor that measures several types of data during the test of a tire, the most important one being the forces and moments in three mutually perpendicular direction. The hub has a high sampling frequency of 160 Hz leading to a need for filtration of noise and averaging of data before gaining insights about the results in the postprocessing stage. The longitudinal force measured by the Kistler sensor represents the drawbar pull if the calibration is performed according to proprietary standards. In a prior study conducted at the lab (Mousavi and Sandu, 2020) the calibration of the sensor when the tire was free rolling on ice was performed resulting in a considerable reduction of the resistive forces and providing insights only into the tractive forces. Though this method is useful for analysis of the tractive performance, the tire in real-life conditions faces a combination of tractive and resistive forces i.e., the drawbar pull and hence the proprietary method of calibration of the Kistler sensor is used in this work.

3.1 Steps for experimental testing

The creation of the ice-bed for testing was done in several stages as follows:

1. Placing the U-channels inverted on the side brackets of the upper level of the chamber and covering it with two layers of plastic tarp and fixing it to the sides of the chamber in a way as to not obstruct the movement of the carriage.
2. Placing a layer of insulation foam by cutting it to the sizes required in order to fit the inner dimensions of the chamber. The foam panels are then fixed with respect to each other and the frame by applying a tape between the panels followed by another layer of plastic tarp on top of the foam, fixed again to the chamber frame.
3. Rolling out the tubular heat exchanger system available on top of the plastic tarp and avoiding overlapping of the tubes in the vertical direction and completing the connections to the inlet and outlet pipes of the chiller. The inlet and outlet pipes are shielded from the external environment by using Rockwool insulation layer.
4. The agent responsible for the exchange of heat is a 50% ethylene glycol solution. The chiller can be set to a certain target temperature and it has a feedback mechanism by virtue of a thermocouple that should be placed on top of the ice surface to control the operation of the chiller.
5. After an initial warm-up of 24 hours, tap water is sprayed at a constant rate of about 2 mm every 2 hours for several days in order to achieve an ice bed thickness of about 3 inches. This rate was found to be optimal for

the compressive strength of ice during previous investigations (Bhoopalam et al., 2015a; Jimenez and Sandu, 2020) at the lab rather than filling the chamber with water and allowing it to freeze thereafter.

6. In order to have a uniform surface roughness of ice, which is known to impact the friction (Lahayne et al., 2016), the clearing of any ice flakes or previous run tire traces on the ice surface was done using the tools available in the lab.

The tires were prepared before the testing phase by undertaking several steps rather than using them in the new condition. The steps undertaken were as follows:

1. **Wearing of tires**: The 16 tires chosen had their vent spews / protuberations removed. This was followed by mounting and running the tires on a vehicle for 100 km. with rotations of the tires after every 25 km. This was done to ensure uniform wear occurred on the tires. This was followed by a period of 3 days during which the tires were left untouched**.** This preparation process is similar to the ASTM standard for single wheel testing on ice (ASTM F1805-20, 2020).

2. **Fixing thermocouples in the grooves of the tires**: The K-type thermocouples (size: ϕ3 mm * 20 mm) were chosen and fixed in the grooves of the tires using two types of silicone (Jimenez and Sandu, 2020). The smaller size chosen was compatible to be accommodated in the characteristic tread pattern of a winter tire without damaging the thermocouple. The drawback of this method though is that the accuracy of the thermocouples is ±2.2°C and the least rate of data transmission by the data loggers to the computers is 10 seconds, which could lead to reservations about the accuracy of the rise in temperature measured experimentally. One of the tires after this process is shown in Figure 8.

Figure 8: Tire after fixing of thermocouples in the grooves

The measurement of the effective rolling radius is essential for the estimation of the ladder value to be used in the PicPro software for implementing a certain slip ratio. In the prior work performed in the TMVS Lab (Mousavi et al., 2019), three methods of estimating the effective rolling radius were benchmarked for their accuracy, and pros and cons. Due to the advantage of measuring only the loaded radius of the tire, the method which involves the formulation found in (Rajamani, 2012) was chosen for estimation of the effective radius (r_{eff}) of all the tires. This formulation is shown in eq. (3) where r_L refers to radius under loaded condition, and r_f refers to radius under unloaded condition. This value of an effective radius is used in the slip equation (He et al., 2020) to determine the angular velocity of the tire and subsequently the ladder value to simulate a specific slip ratio.

$$r_{eff} = \frac{sin\left(cos^{-1}\left(\frac{r_L}{r_f}\right)\right)}{cos^{-1}\left(\frac{r_L}{r_f}\right)} * r_f \tag{3}$$

The tires were cooled down to a temperature much below the temperature of the ice surface before every test. This made sure that after completion of the mounting and calibration process, the tire temperature would be in the close vicinity of the ice surface temperature in order to mimic the actual conditions.

3.2 Design of experiments for experimental testing

The design of experiments was created in such a way so that the only factor differing in the tests would be the tread rubber compound of the tires. The chosen values of inflation pressure and normal load were 193 kPa (28 psi) and 4 kN, respectively. There was no variation in the camber and toe angles and they were kept at 0°. As it was found previously that testing of tires at ice temperatures like -10°C would lead to conditions similar to dry friction, the ice temperature chosen was -1°C. Application of slip ratios was done in sets of 3 slip ratios in a test and the final two slip ratios in the same test. The configurations shown in Table 2, were tested twice to make sure the test data had repeatability. The design of the rig allows to test three slip ratios in a single run. Runs 1 and 2 for a specific slip ratio combination were run one after the other so there was not much time difference between them. The initial temperature measured by the thermocouples during both the tests varied a maximum of 1°C during the initial slip ratios (up to 10%) but the variation in the initial temperature of the rubber was maximum 0.5°C for higher slip ratios.

Table 2
Design of experiments

	Rubber comp. A		Rubber comp. B		Rubber comp. C		Rubber comp. D		Rubber comp. E		Rubber comp. F		Rubber comp. G		Rubber comp. H	
Tire	Tire A1	Tire A3	Tire B1	Tire B3	Tire C1	Tire C3	Tire D1	Tire D3	Tire E1	Tire E3	Tire F1	Tire F3	Tire G1	Tire G3	Tire H1	Tire H3
Load (kN)	4	4	4	4	4	4	4	4	4	4	4	4	4	4	4	4
Infl. Pres. (kPa)	193	193	193	193	193	193	193	193	193	193	193	193	193	193	193	193
Slip ratio	0%, 2%, 4%, 6%, 8%, 10%, 12%, 15%, 20%, 25%, 30%, Free Rolling															

4. Results from experimental investigation and discussion

As the ambient temperature is an important parameter affecting the results, as explained in section 2.4, an attempt was made to keep the ambient temperature constant during the testing of all the tires as this is one parameter that cannot be currently controlled in the experimental setup at TMVS lab. The tests on almost all of the tires were conducted when the ambient temperature was about 10-11°C. However, two tires (one each of rubber compounds F and H) were tested at about 6°C. Before delving into the results of the tests, a brief overview of the material properties of the rubber compounds is detailed in this section.

4.1 Properties of rubber compounds

The constituents of the rubber compounds of the tread were not known exactly but some mechanical and thermal properties were available as follows:

1. **Rubber Compound Density**: The density of the rubber compound varied between 1094 kg/m^3 for rubber compound C to 1157 kg/m^3 for the rubber compound H, as shown in Table 3.

Table 3
Density of the rubber compounds

Rubber Compound	Density (kg/m^3)
A	1105
B	1103

C	1094
D	Not Provided
E	1104
F	1139
G	1137
H	1158

2. **Thermal conductivity of the rubber**: The thermal conductivity of the rubber is generally very less than the thermal conductivity of ice and was assumed to be constant for all the rubber compounds in this work (0.3 $Wm^{-1}K^{-1}$).
3. **Rubber's specific heat capacity** (J/(g.K)): This property was known at various temperatures for 5 rubber compounds. The excerpt of the properties is shown in Table 4.

Table 4
Excerpt of the specific heat capacity values of the rubber compounds at different temperatures

Temp. (℃)	A	B	C	D	E	F	G	H
-5	Not Available	1.84	2.03	2.09	Not Available	2.18	2.09	Not Available
0		1.88	2.14	2.26		2.28	2.26	
5		1.92	2.18	2.29		2.30	2.29	

4. **Stiffness related properties**: The loss modulus, storage modulus, dynamic modulus, and the tangent of the phase difference at various temperatures were available for many of the rubber compounds. The dynamic modulus is a parameter required for the simulation-based study for estimating the height of water film and a rise in temperature and was available for 7 of the rubber compounds. Excerpts of the various properties are presented from Table 5 - Table 8.

Table 5
Loss modulus at different temperatures for various rubber compounds

Temp (℃)	E'' (in MPa)							
	A	B	C	D	E	F	G	H
-5.6	Not Available	0.808	0.839	Not Available	Not Available	Not Available	1.115	1.669
-2.7		0.765	0.771				0.992	1.54
0.4		0.587	0.762				0.983	1.328

Table 6
Storage modulus at different temperatures for various rubber compounds

Temp (°C)	E' (in MPa)							
	A	**B**	**C**	**D**	**E**	**F**	**G**	**H**
-5.6	Not Available	3.495	4.556	Not Available	Not Available	Not Available	6.489	7.977
-2.7		3.401	4.197				6.184	7.568
0.4		3.137	4.153				6.03	7.115

Table 7
Dynamic modulus of rubber at different temperatures for various rubber compounds

Temp (°C)	E* (in MPa)							
	A	**B**	**C**	**D**	**E**	**F**	**G**	**H**
-5.6		3.587	4.633	Not Available			6.584	8.149
-2.7		3.486	4.268				6.263	7.723
0.4	4.21	3.191	4.222		5.26	4.87	6.11	7.238

Table 8
Tangent of phase different at different temperatures for various rubber compounds

Temp (°C)	tanδ							
	A	**B**	**C**	**D**	**E**	**F**	**G**	**H**
-5.6	Not Available	0.231	0.184	Not Available	Not Available	Not Available	0.172	0.209
-2.7		0.225	0.184				0.16	0.204
0.4		0.187	0.184				0.163	0.187

4.2 Results considering the variation in the rubber compound

The data collected by the Kistler sensor was filtered using an equ-ripple filter and averaged for the drawbar pull for a certain slip ratio. The performance curves presented in this section are based on the drawbar pull coefficient i.e. the normalized longitudinal force with respect to the normal load. The presented curves show an average value of both the runs with the variation in the two runs depicted by the error bar. Generally, at slip ratios higher than 10% - 12%, an intermittent sticking of the tire occurs when it moves on ice, and this is discernible while testing a single tire on an equipment such as the Terramechanics Rig. This effect was seen in all the cases except for the tires of rubber compound A. In certain cases, due to change in the ambient temperature, aging effect, change in surface roughness (which cannot be measured in the lab), or the

possibility that the tread rubber compound is not exactly identical, there is variation in the performance curves of both the tires of same rubber compound in some cases, which led to the need of presenting the results of an individual tire separately.

1. **Rubber compound A**: An approximately identical DPC-slip curve was depicted by both the tires of this rubber compound wherein the maximum value of the DPC was about 0.24 on average and the maxima were at 6% slip ratio, as shown in Figure 9 and Figure 10.

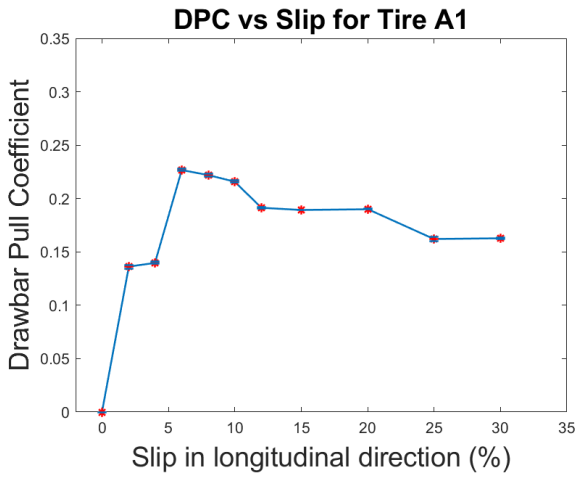

Figure 9: Performance curve for tire A1 depicting variation in DPC with variation in slip ratio

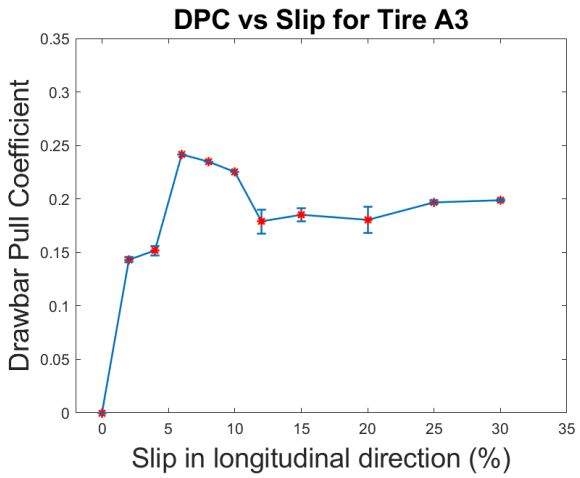

Figure 10: Performance curve for tire A3 depicting variation in DPC with variation in slip ratio

2. **Rubber compound B**: Tires of rubber compound B, too showed a maxima at 6% slip ratio averaging about 0.27, and the results are presented in Figure 11 and Figure 12.

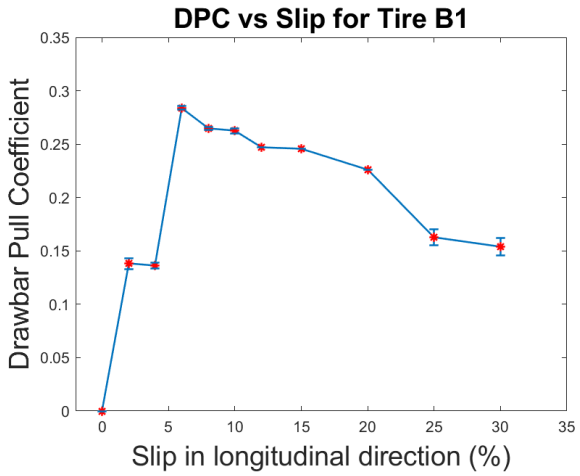

Figure 11: Performance curve for tire B1 depicting variation in DPC with variation in slip ratio

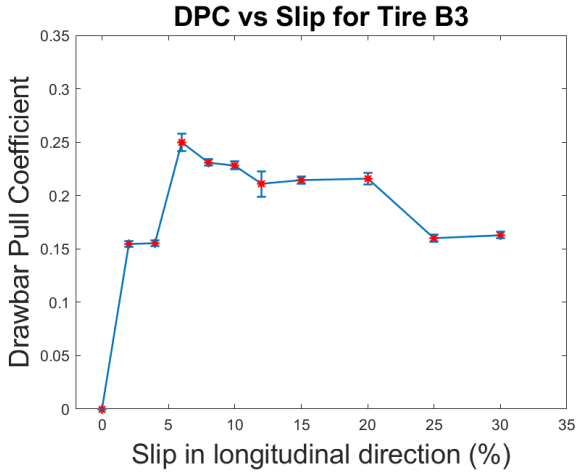

Figure 12: Performance curve for tire B3 depicting variation in DPC with variation in slip ratio

3. **Rubber compound C**: The average peak drawbar pull coefficient was 0.16 for rubber compound C's tires as presented in Figure 13 and Figure 14.

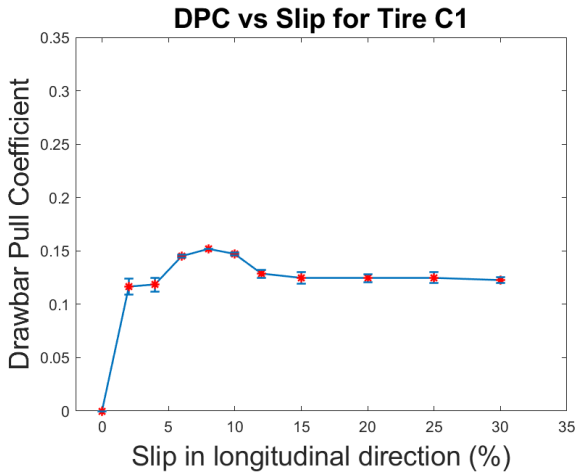

Figure 13: Performance curve for tire C1 depicting variation in DPC with variation in slip ratio

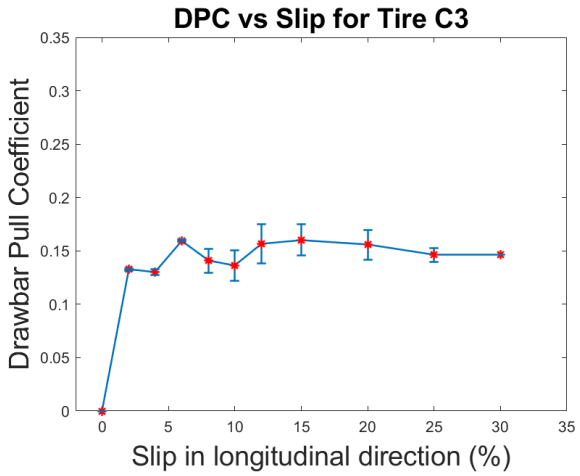

Figure 14: Performance curve for tire C3 depicting variation in DPC with variation in slip ratio

4. **Rubber compound D**: The peak value of the drawbar pull coefficient in the rubber compound D's tires was about 0.29. The peak, however, occurred at 6% slip ratio for tire D1 (Figure 15) and 12% for tire D3 (Figure 16). This inconsistency was noticeable even after several retesting rounds. We postulate that there is a possibility that both the tires are not exactly identical in the tread rubber compound or there may have been a slight deviation in the processes followed during the manufacturing of the tires as no other valid justification for this behavior exists.

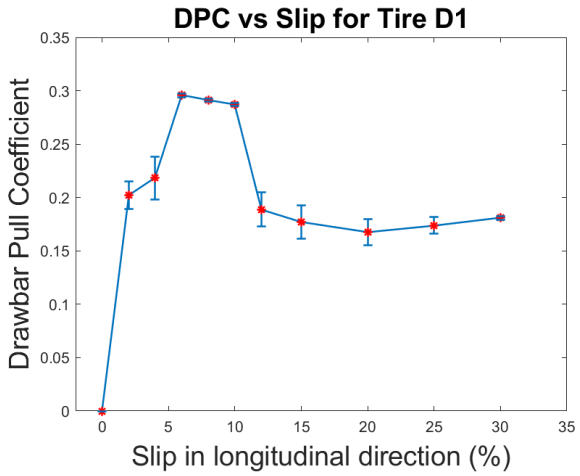

Figure 15: Performance curve for tire D1 depicting variation in DPC with variation in slip ratio

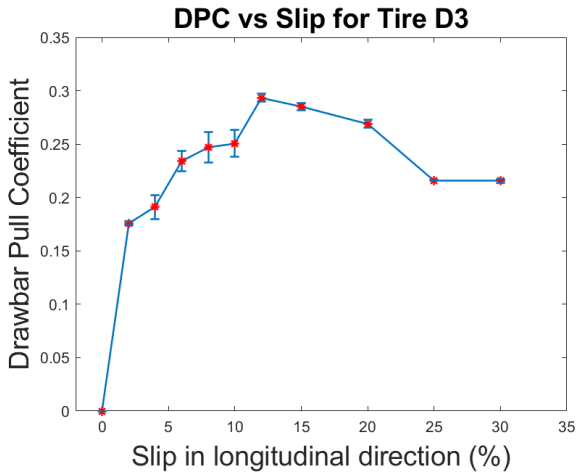

Figure 16: Performance curve for tire D3 depicting variation in DPC with variation in slip ratio

5. **Rubber compound E**: The average peak DPC value for tires of rubber compound E was 0.2. For tire E1, an upward trend in the curve is found at 12% slip ratio which could be either due to the rubber compound (similar to rubber compound D) or minor change in the ambient temperature during the tests of the 12-15-20 slip ratios. But except for this, the curves of both tires match in both cases so the chances of variation in rubber compound are less.

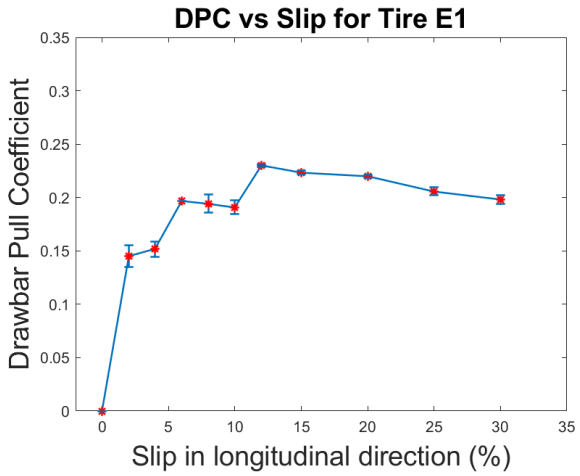

Figure 17: Performance curve for tire E1 depicting variation in DPC with variation in slip ratio

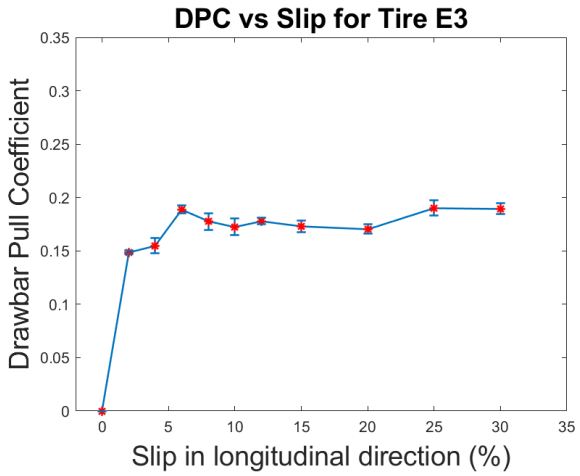

Figure 18: Performance curve for tire E3 depicting variation in DPC with variation in slip ratio

6. **Rubber compound F**: The ambient temperature could not be maintained and hence in the case of tire F1 was about 6°C whereas for tire F3 it was 10°C. This led to a deviation in the value of the maximum drawbar pull experienced by the tires as shown in Figure 19 and Figure 20.

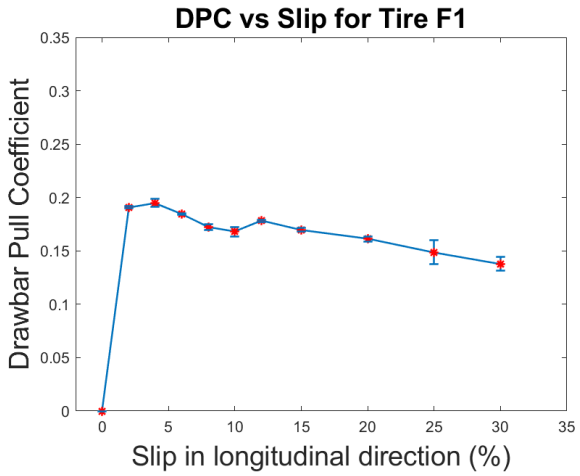

Figure 19: Performance curve for tire F1 depicting variation in DPC with variation in slip ratio

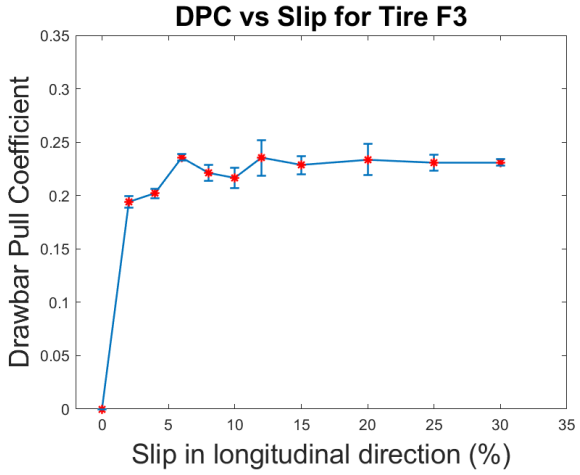

Figure 20: Performance curve for tire F3 depicting variation in DPC with variation in slip ratio

7. **Rubber compound G**: The tires of rubber compound G had similar trends and peaked at 6% slip ratio with the average value of the peaks being about 0.19.

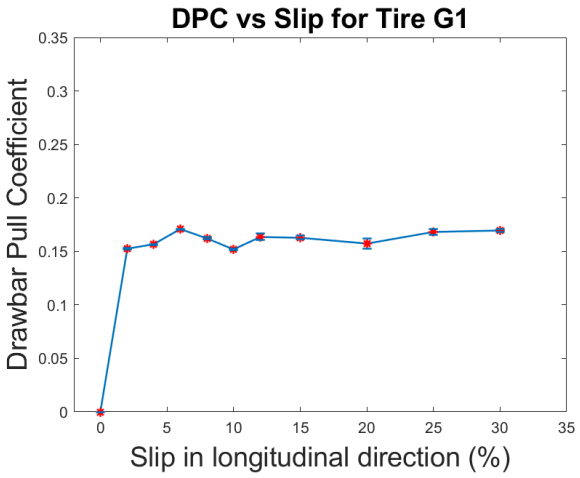

Figure 21: Performance curve for tire G1 depicting variation in DPC with variation in slip ratio

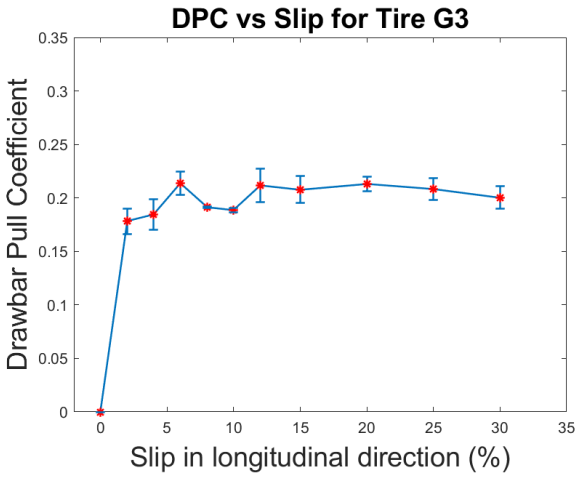

Figure 22: Performance curve for tire G3 depicting variation in DPC with variation in slip ratio

8. **Rubber compound H**: In the case of rubber compound H, tire H1 was tested at about 11°C ambient temperature but in the case of tire H3, the ambient temperature was 6°C. Due to a failure of the setup during the testing, the slip ratios greater than 12% for tire H1 had to be tested at an ambient temperature of approximately 8°C, and hence Figure 23 shows the values that would have been the logical possibility of DPC values in this region. The DPC-slip curve of tire H3 is presented in Figure 24.

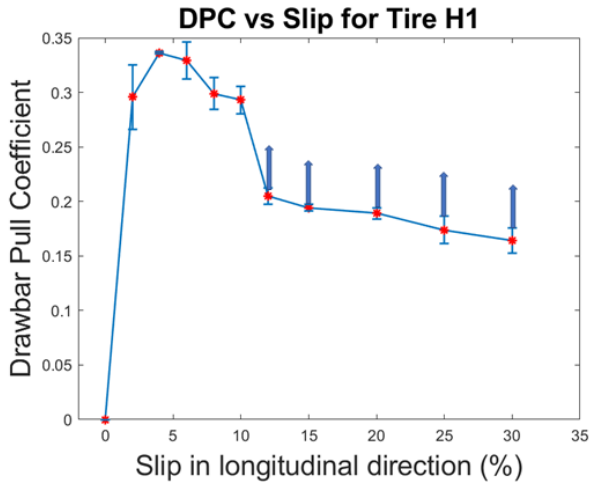

Figure 23: Performance curve for tire H1 depicting variation in DPC with variation in slip ratio

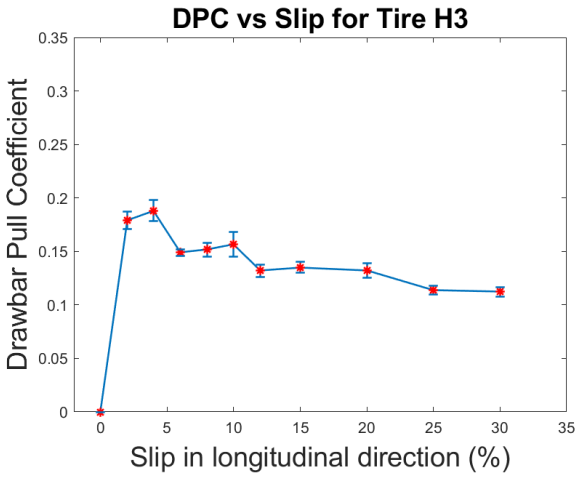

Figure 24: Performance curve for tire H3 depicting variation in DPC with variation in slip ratio

4.3 Effect of ambient temperature on tire performance curves

As explained earlier the ambient temperatures during the testing of tires of rubber compounds H and F were the difference and the performance curves got affected as explained in section 4.2. The effect of the drop in positive ambient temperature is more pronounced in the case of rubber compound H as compared to rubber compound F as shown in Figure 25. The drop in ambient temperature also affected the equivalent coefficient of friction i.e. the number of resistive forces measured in the free-rolling condition normalized with respect to the normal load (Figure 26). The percentage reduction in maximum DPC

can also be considered as a function of the rubber compound properties as this reduction was 44% for rubber compound H but only 17% for rubber compound F for the same drop in ambient temperature.

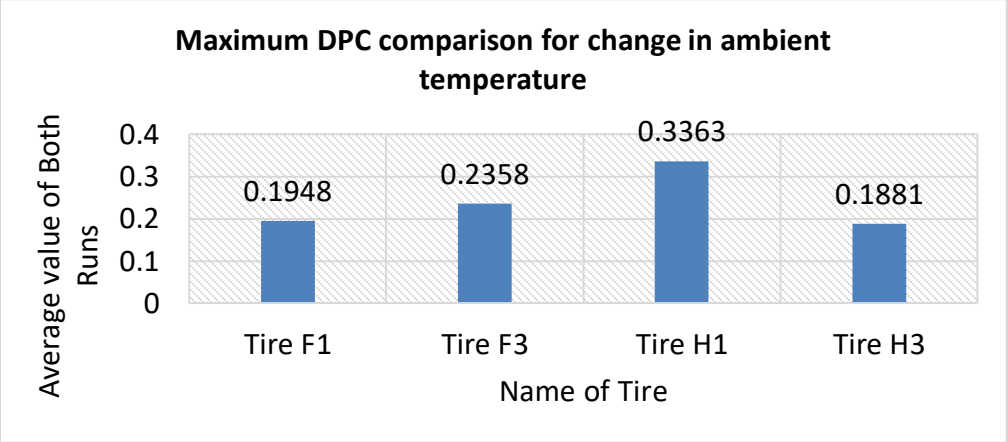

Figure 25: Comparison of maximum DPC with a change in ambient temperature

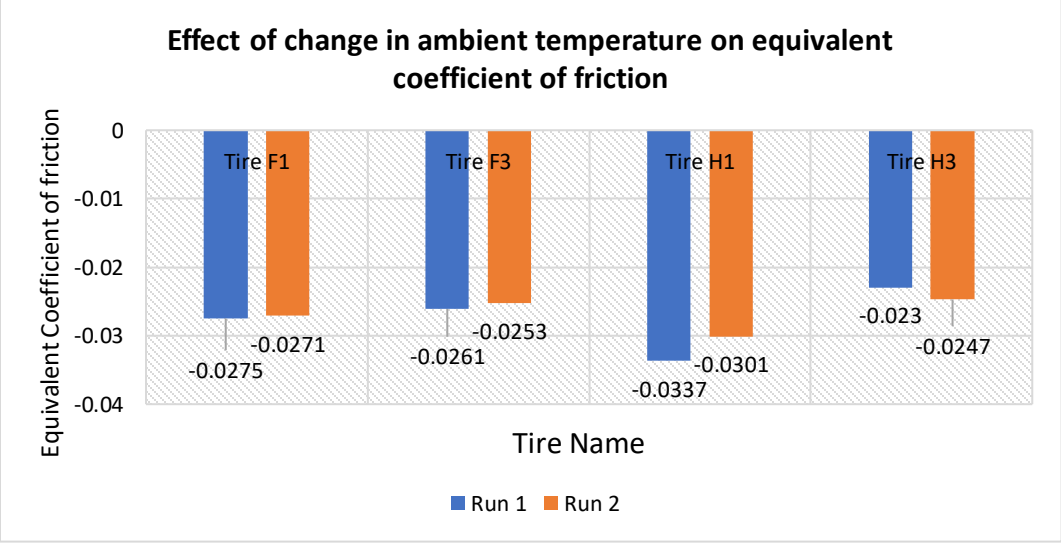

Figure 26: Effect of change in ambient temperature on the equivalent coefficient of friction

4.4 Effect of aging

The tire 3 of rubber compounds B, C, and G were tested earlier in the winter of 2019 following the same procedures. The operational parameters for these tires were the same except for inflation pressure. The inflation pressure of 144.79 kPa was chosen for the tests conducted in 2019 while for the tests conducted in 2020 the inflation pressure was 193 kPa. Hence a direct comparison for the effect of aging only on the drawbar pull coefficient was not possible.

As it can be seen from Figures 27, 28, and 29 there is a reduction in the performance of all three tires tested after one year of aging and with an increase in the inflation pressure from 144.79 kPa to 193 kPa. Based on the previous results obtained by the authors from another study (Mousavi et al., 2019), approximately 6.5% decrease in the value of drawbar pull for free rolling condition was observed when inflation pressure increased from 144.79 kPa to 193 kPa (Figure 30) in the study conducted in 2019.

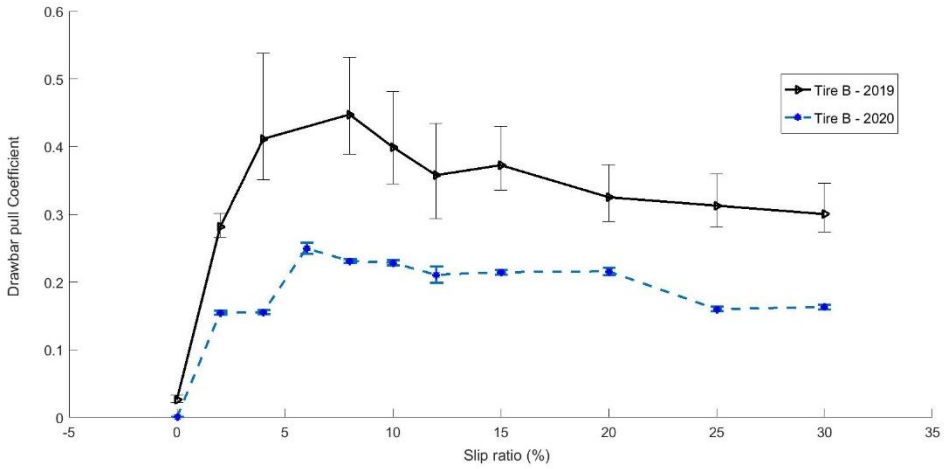

Figure 27: Performance curve for tire B3 depicting variation in DPC with variation in slip ratio for tests conducted in 2019 and 2020

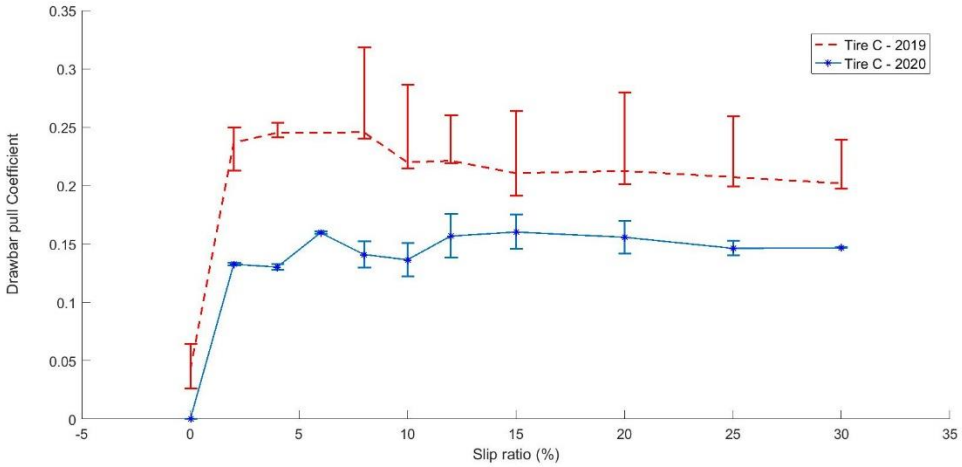

Figure 28: Performance curve for tire C3 depicting variation in DPC with variation in slip ratio for tests conducted in 2019 and 2020

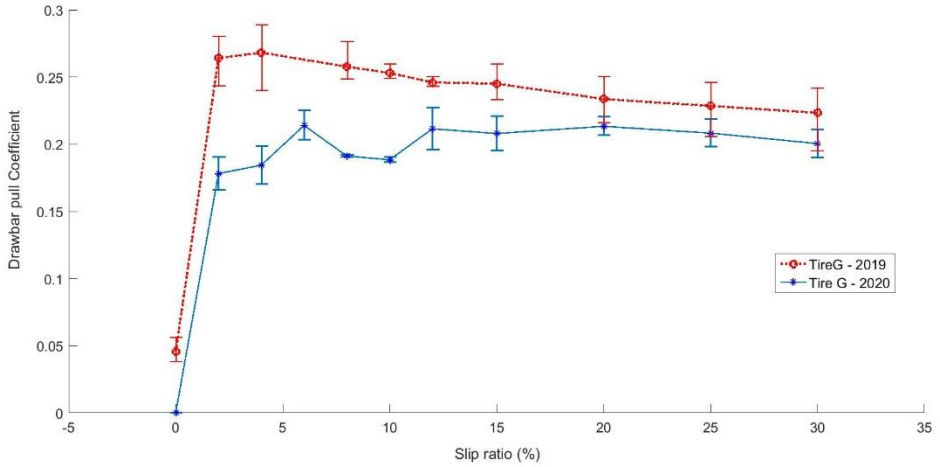

Figure 29: Performance curve for tire G3 depicting variation in DPC with variation in slip ratio for tests conducted in 2019 and 2020

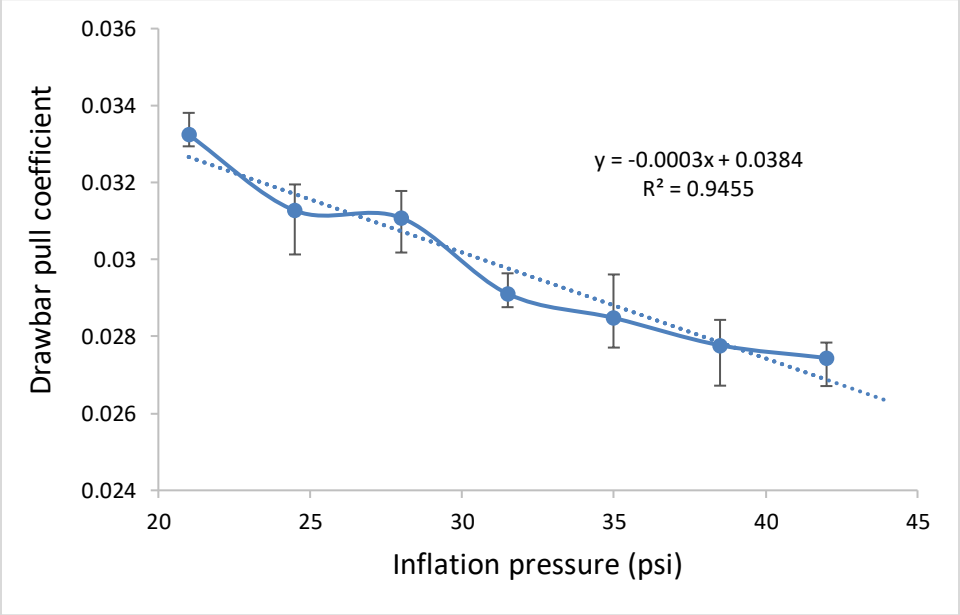

Figure 30: Variation in drawbar pull coefficient versus percentage of nominal inflation pressure for free rolling condition of tire in contact with ice. Adapted from the results in (Mousavi et al., 2019).

4.5 Effect on the normalized resistive forces

The equivalent coefficient of friction calculated from the free-rolling tests for all the tires was plotted as a histogram for comparative analysis in Figure 31. Please note that the histogram takes into account only the tires of rubber compounds F

and H which were tested at the same ambient temperature as tires of other rubber compounds. It can be seen that rubber compound C had the highest resistive forces per unit normal load whereas rubber compound F had the least.

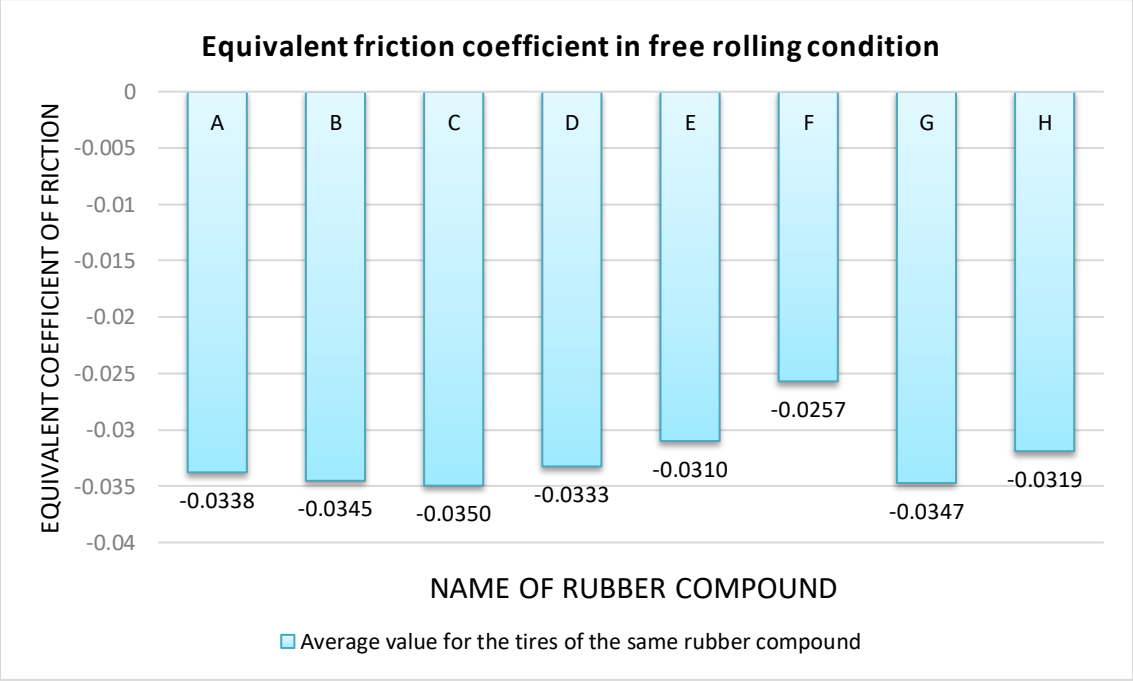

Figure 31: Equivalent coefficient of friction for all the rubber compounds

4.6 Measured rise in temperature in the tread

As the tires were outfitted with thermocouples, the rise in temperature during the tests was measured and averaged for a duration of 20 seconds for every slip ratio. A histogram was plotted (neglecting tire H3 and tire F1) and is presented in Figure 32 for the free rolling condition. By considering the specific heat capacity properties available for 5 of the rubber compounds, it can be generalized that a lower specific heat capacity value would lead to a higher rise in temperature. Building upon this statement it can be postulated that rubber compound H would have the lowest value of specific heat capacity but a more accurate measurement should be performed or the logging time should be reduced in order to arrive better deductions from the measurements.

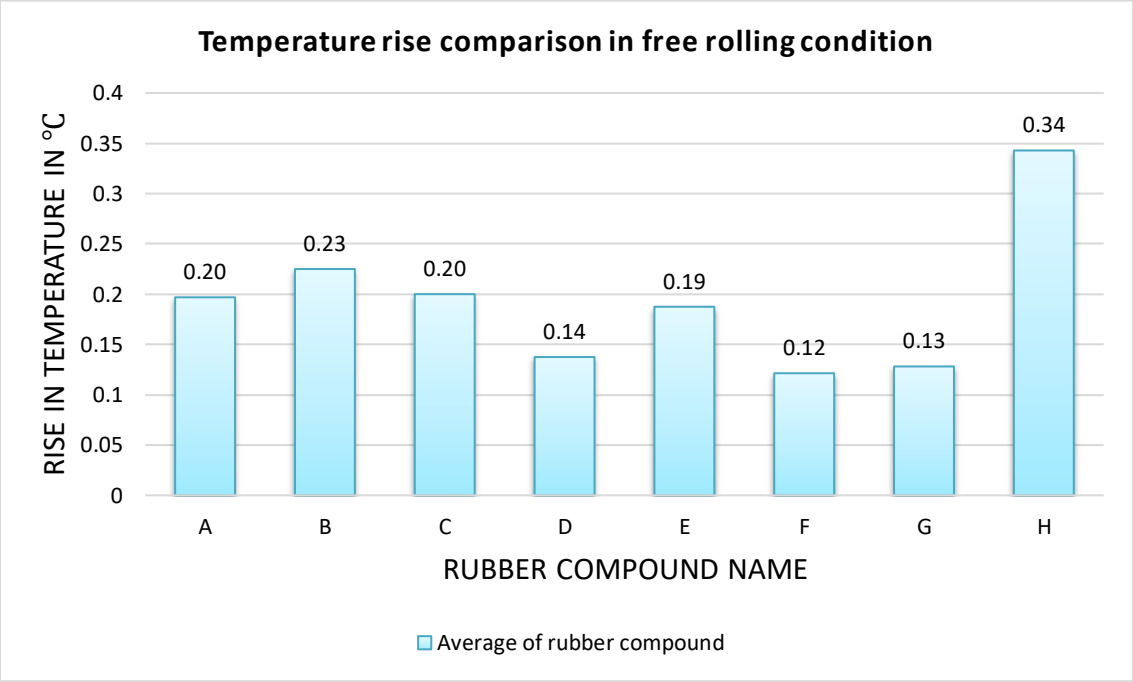

Figure 32: Comparison of rise in temperature measured experimentally in the free rolling condition

4.7 Summary of results from experimental testing

The results of the experimental testing explained earlier in section 4, can be summarized as follows:

1. The rubber compound C is not a good candidate for winter tires on ice as the tires of rubber compound C performed the worst in the amount of drawbar pull and also had the largest resistive forces.
2. Rubber compound G would be second to last in this order based on the same two parameters of DPC and resistive forces.
3. The effect of the rubber compound was most pronounced in the lower slip region. This is also the region in which vehicles operate most of the time whereas in the higher slip region the drawbar pull kind of plateaued and the values of DPC at 30% slip ratio were in a small range of each other.
4. The order of performance, considering the maximum DPC as the criteria leads to the following order:

   H > D > B > A > F > E > G > C

5. The results provided in this section were for tests conducted at low speeds whereas the consistency of this order of performance at high speeds needs to be investigated.
6. Though the lower stiffness is supposed to yield better results as explained in section 2.3, this trend was not followed as the rubber compound H has a higher dynamic modulus and higher density and yet performed the best. Thus, we can

conclude that the stiffness properties of the rubber cannot be singled out as the responsible parameter when testing a tire and further examination could lead to better insights.

5. Parametrization using the Genetic Algorithm technique

The '*Magic Formula Tire Model*' is one of the most recognized tire models of empirical nature (Pacejka and Bakker, 1992). In general, the model is capable of estimating the longitudinal force (F_x), lateral force (F_y), and aligning moment (M_z) characteristics in pure and combined slip (s) conditions. Based on the experimental testing approach followed in this work, only the longitudinal force characteristics were considered, which are presented in eqns. (4) to (6). Eqns. (5) and (6) have factors like *'S_v'* and *'S_h'* which are used to allow for the curve to be able to accommodate a shift in the intercepts at the force and slip axes. The four factors in eq. (4) namely, the stiffness (B), shape (C), peak value (D), and curvature factors (E) were parametrized for the testing regime. Normally, the data to parametrize the Magic Formula for a tire in a specific condition is done at high velocities, although this is not possible in the TMVS laboratory. An accurate depiction of the parameters, by including the camber angle effects during steady-state cornering requires a high number of tests to be conducted on each tire (Van Oosten, 1999). Thus, the results of the parametrization should be viewed simply as an attempt to find the effects on the various parameters but the values found were not validated.

$$F_x(s) = D\ sin\ (C * (B * s\ -\ E(B * s\ -\ (B * s))))\ ) \tag{4}$$

$$F_{long.}(S) = F_x(s) + S_v \tag{5}$$

$$s = S + S_h \tag{6}$$

The Genetic Algorithm (GA) has several advantages over the classical methods of parametrization, the most important being that it is not as sensitive to the initial guess as compared to an algorithm like the least-squares technique. It is based on the theories of evolutionary biology especially the principles of genetics and natural selection. It attempts to optimize a set of parameters instead of the individual parameters (Goldberg, 1989). A randomly generated population within the bounds set is generated and its cost function is calculated. The value of the cost functions such evaluated is then used to determine the set of parents for the reproduction process. During the reproduction, the first step consists of a crossover to develop the genes (parameters) of the offsprings which is governed by the crossover probability. After crossover, the mutation process is implemented to add some variation to the genes, and thus the mutation probability should be less as it may lead to oscillations

in the region of the minima instead of steadily approaching the minima. The same process is then repeated for the individuals of the next generation to decide the best parents for reproduction. This cycle continues until the stop condition is achieved or the number of iterations are completed. For the purpose of this work, the Genetic Algorithm optimization was coded using the MATLAB software. The range of the genotype (individual factors) in the chromosome of an individual was considered to be varying between -100 and 100 for genes of factors B & C. The range for factors D was 0 to 1000 whereas for factor E the range was -10 to 10. Fitness for reproduction in the next generation was considered as the children of the current generation that led to the lowest cost function whereas the mutation probability added variations before reproduction of the next generation. As the data points available were not very much, attempt of optimization was made with the total population of 50 as well as 100 but the final results considered were of 100 population as this would provide a more varied distribution for the individuals. The values of the conditions set for the optimization process are shown in Table 9.

Table 9
Set of parameters for the optimization process using Genetic Algorithm

Sr. No.	Parameter of the algorithm	Set Value
1	Number of iterations	40000
2	Crossover probability	0.4
3	Mutation probability	0.05
4	Population	100
5	Stop condition	5% of normal load

The optimization process was performed for the average value of both the runs of a specific tire as well as with respect to both the runs with the goal being the minimization of the cost function. The cost function was defined as the root mean squared error between the predicted and measured values of the drawbar pull for a certain case. The values found for the factors of a specific tire were nearly the same in both cases, although the optimization with the average of runs yielded a lower cost function. The algorithm ran for all the generations in nearly all the cases which could be due to the prescribed stop condition being too harsh or due to uncertainties in the collected experimental data to effectively match the theoretical Magic Formula. The results of the optimization process for all the tires with optimization against the average value of the runs as the goal are presented in Table 10.

Table 10
Optimized parameters against the average of both runs of the Magic Formula Tire Model

Sr. No.	Tire Name	(B)	(C)	(D)	(E)	Final value of the cost function (kN)
1	Tire A1	0.1715	1.6822	0.8521	0.1046	0.0664
2	Tire A3	0.2056	1.4604	0.8721	-0.7359	0.0845
3	Tire B1	0.1044	1.9875	1.0765	-0.0922	0.0973
4	Tire B3	0.1635	1.8886	0.9223	0.5535	0.0780
5	Tire C1	0.3819	1.5159	0.5599	0.6140	0.0324
6	Tire C3	2.8855	0.8303	0.6395	0.8012	0.0330
7	Tire D1	0.1915	1.7578	1.1277	-0.6180	0.1133
8	Tire D3	0.5147	0.7461	1.1266	-0.5194	0.1036
9	Tire E1	0.5355	0.8554	0.9090	0.5036	0.0540
10	Tire E3	1.5428	0.5446	0.9859	0.3642	0.0321
11	Tire F1	0.9888	1.6929	0.7726	0.8855	0.02
12	Tire F3	1.5521	0.7556	1.0173	0.5239	0.0279
13	Tire G1	3.6132	0.8672	0.6740	0.6060	0.0211
14	Tire G3	3.8437	0.4147	0.8845	0.6732	0.0337
15	Tire H1	0.2980	1.8271	1.3976	-0.0627	0.0651
16	Tire H3	0.7007	1.6795	0.7308	0.5614	0.0309

The values of the optimized parameters in the case of tires of rubber compound A (which had no effect of aging or ambient temperature variation) are nearly the same though the curve of tire A1 is better fitting to the nature of the formulation which is evident by a lower value in the final cost function. The performance curve of the tire A3 and reduction in the values of the cost function with the number of iterations are presented in Figure 33 and Figure 34 respectively.

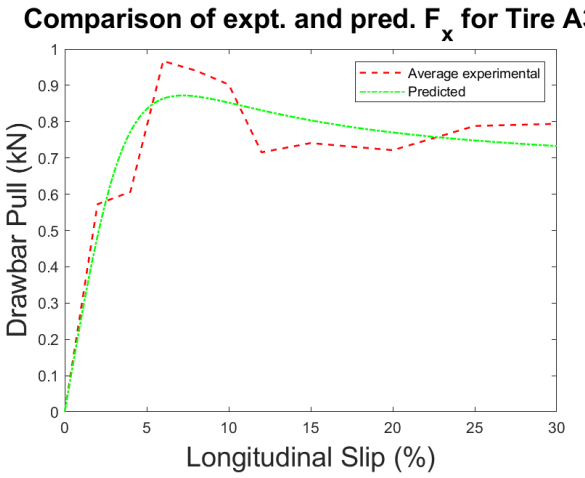

Figure 33: Parametrized Magic Formula curve against average of experimental results for tire A3

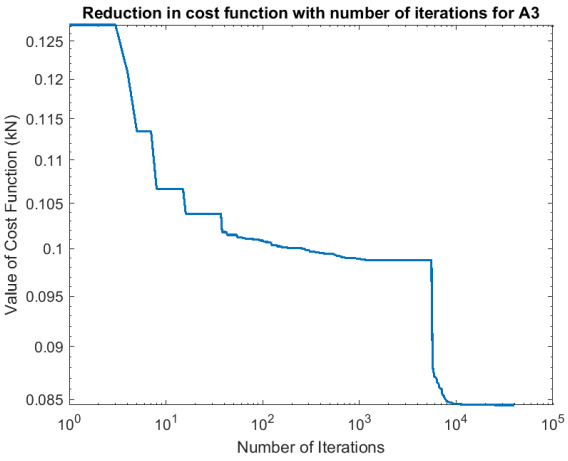

Figure 34: Reduction in the value of cost function with an increase in the number of generations for tire A3

The uncertainty in the data collected at higher slip ratios in some conditions led to the parametrized curve following a trend that is more typical of the tire brush model as in the case of tire C3 as shown in Figure 35. The major reason for this abnormality is that the algorithm attempts to reduce the overall value of cost function with respect to all the data points provided. A similar evaluation of the parameters by optimizing against both the runs of the tires yielded the parameters detailed in Table 11. In the case of both the approaches, it can be deduced that the ambient temperature not only affects the peak value factor but also the stiffness factor when we consider rubber compounds F and H. In the case of tire F3, a discernible plateau after the peak region does not exist and hence the shape and curvature factors can get affected by this as can be seen in the results. In the case of tires of rubber compound B, and C, which have the aging effect, a rise in the value of the stiffness factor and the angle at the origin can be concluded as an effect of aging.

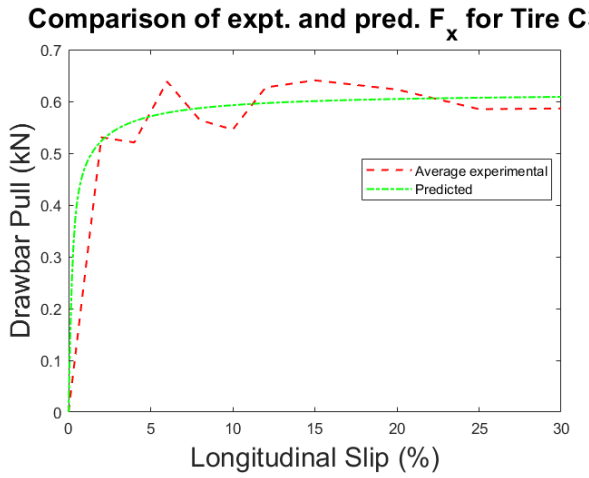

Figure 35: Parametrized Magic Formula curve against average of experimental results for tire C3

Table 11
Optimized parameters of the MFTM against both runs of all the tires

Sr. No.	Tire Name	(B)	(C)	(D)	(E)	Final value of the cost function (kN)
1	Tire A1	0.1711	1.6769	0.8529	0.0725	0.0665
2	Tire A3	0.2086	1.4572	0.8698	-0.6831	0.0874
3	Tire B1	0.1044	1.9775	1.0772	-0.1326	0.0985
4	Tire B3	0.1634	1.8942	0.9223	0.5625	0.0808
5	Tire C1	0.3829	1.5136	0.5597	0.6111	0.0364
6	Tire C3	2.2198	0.9243	0.6192	0.8176	0.0523
7	Tire D1	0.1917	1.7584	1.1275	-0.6103	0.1212
8	Tire D3	0.5404	0.5772	1.3182	-0.9837	0.1082
9	Tire E1	0.5629	0.8074	0.9312	0.4754	0.0579
10	Tire E3	1.0662	0.9462	0.7405	0.6589	0.0388
11	Tire F1	0.6686	1.8879	0.7716	0.9318	0.0257
12	Tire F3	1.5725	0.7465	1.0243	0.5199	0.0445
13	Tire G1	3.5299	0.7835	0.7	0.4508	0.0225
14	Tire G3	2.9349	0.6237	1.0138	0.6594	0.0530
15	Tire H1	0.2945	1.8227	1.4010	-0.1173	0.0840
16	Tire H3	0.6291	1.6589	0.7353	0.3998	0.0405

6. Conclusions and directions for future research

An experimental investigation focusing on the effect of the tread rubber compound in winter tires was undertaken by considering two tires each of eight different rubber compounds. The winter tires chosen were identical in design and all the other aspects except for the composition and properties of the rubber compound. The ice bed was at -1°C throughout the tests of all the tires.

The order of performance was found to be changing with the sole effect of the rubber compound coming into the play at the low speeds tested. The validity of the order of performance at higher speeds needs to be investigated. The maxima of the DPC-slip curve were found to be occurring at 6% or 8% slip ratio for the majority of the tires. As some material properties for four of the rubber compounds were not available, a direct one-to-one correlation of the performance with the individual properties is not possible but the investigation has helped in concluding that the lower stiffness of the rubber cannot be a factor that can be held responsible for an increase in the performance (available friction) of the tire. Rubber compound H, having the highest dynamic modulus and density performed the best in the experimental investigation whereas rubber compound C had the lowest DPC and highest equivalent coefficient of friction. The investigation has also led to conclusive evidence that amongst the rubber compounds considered, the tread rubber compound could affect the maximum DPC by a factor of two when comparing the best and least performances. Another worthy conclusion is that the tread rubber compound affects the tire performance the most in the low slip region whereas in the high slip region all the tires tend to plateau within a small range of DPC values. Now, though most of the vehicles generally operate in the low slip region underlining the importance of this finding, during emergency braking or sudden maneuvers, the reliance on the tread rubber compound effect is non-existent. The experimentally measured temperature rise in the tread of the tires has proved that a lower specific heat capacity would yield a higher rise in temperature in the contact patch.

An attempt to parametrize the Magic Formula tire model led to interesting insights in the effect of tread rubber compound, aging, and ambient temperature on the individual parameters of the MFTM. It was found that the ambient temperature affects the stiffness factor and peak value factor whereas the aging of a tire leads to an increase in the stiffness factor and angle at the origin of the aged tire.

For future work, it is essential to analyze the contents of the tread rubber with respect to the change in the performance of the tire. In many studies found in literature like (Hiramatsu et al., 1991; Okel and Rueby, 2016; Weng et al., 2020), it has been found that increasing the filler material like silica or improving its dispersion in the matrix of the rubber can help reduce the rolling resistance of the tire and improve the wet traction of the tire. The addition of petroleum resins, too, can improve

wet traction. Such effects cannot be directly judged based on the material properties of the rubber compound that were available. In order to have an in-depth knowledge of the effect of tread rubber compound, the ingredients of the tread rubber need to be taken into consideration in detail. For future studies, control over the ambient temperature during testing will help reduce the uncertainties in the experimentally collected data.

Acknowledgments

This study has been partially supported by Sumitomo Rubber Industries Ltd. and Terramechanics, Multibody and Vehicle Systems Laboratory at Virginia Tech. The authors would like to thank the guidance and support provided by Dr. Toshio Tada.

References

ASTM F1805-20, 2020. Standard Test Method for Single Wheel Driving Traction in a Straight Line on Snow-. ASTM International, West Conshohocken, PA. https://doi.org/10.1520/F1805-20

Bhoopalam, A.K., Sandu, C., Taheri, S., 2015a. Experimental investigation of pneumatic tire performance on ice: Part 1 - Indoor study. J. Terramechanics 60, 43–54. https://doi.org/10.1016/j.jterra.2015.02.006

Bhoopalam, A.K., Sandu, C., Taheri, S., 2015b. Experimental investigation of pneumatic tire performance on ice: Part 2 - Outdoor study. J. Terramechanics 60, 55–62. https://doi.org/10.1016/j.jterra.2015.03.001

Blundell, M., Harty, D., 2004. The Multibody Systems Approach to Vehicle Dynamics. Elsevier Butterworth-Heinemann, Burlington, MA.

Goldberg, D.E., 1989. Genetic Algorithms in Search, Optimization and Machine Learning. Addison-Wesley Publishing Company Inc.

Greenwood, J.A., Williamson, J.B.P., 1966. Contact of nominally flat surfaces. Proc. R. Soc. London. Ser. A. Math. Phys. Sci. 295, 300–319.

He, R., Sandu, C., Mousavi, H., Shenvi, M.N., Braun, K., Kruger, R., Els, P.S., 2020. Updated standards of the international society for terrain-vehicle systems. J. Terramechanics 91, 185–231. https://doi.org/10.1016/j.jterra.2020.06.007

Hiramatsu, K., Kamamizu, K., Komai, M., Okazaki, T., Takino, H., 1991. Rubber and collagen-fiber blends for studless winter tire applications. Rubber World 204, 38–43, 45.

Isitman, N.A., Kriston, A., Fülöp, T., 2017. Role of Rubber Stiffness and Surface Roughness in the Tribological Performance on Ice. Tribol. Trans. 61, 295–303. https://doi.org/10.1080/10402004.2017.1319002

Jimenez, E., Sandu, C., 2020. Experimental Investigation of the Tractive Performance of Pneumatic Tires on Ice. Tire Sci. Technol. 48, 22–45.

Jung, H.C., Park, W.C., Jeong, K.M., 2018. Finite Element Analysis of Tire Traction Using a Rubber-Ice Friction Model. Open J. Appl. Sci. 08, 495–505. https://doi.org/10.4236/ojapps.2018.811040

Khan, A.K., Sandu, C., 2017. Design and Manufacturing of a Clutch and Brake System for Indoor Tire Testing, in: Proceedings of the ASME 2017 International Design Engineering Technical Conferences and Computers and Information in Engineering Conference IDETC/CIE 2017. pp. 1–10.

Klapproth, C., Kessel, T.M., Wiese, K., Wies, B., 2016. An advanced viscous model for rubber-ice-friction. Tribol. Int. 99, 169–181. https://doi.org/10.1016/j.triboint.2015.09.012

Lahayne, O., Pichler, B., Reihsner, R., Eberhardsteiner, J., Suh, J., Kim, D., Nam, S., Paek, H., Lorenz, B., Persson, B.N.J., 2016. Rubber Friction on Ice: Experiments and Modeling. Tribol. Lett. 62, 1–19. https://doi.org/10.1007/s11249-016-0665-z

Moore, D.F., 1975. The Friction of Pneumatic Tires.

Motamedi, M., Taheri, S., Sandu, C., 2016. Rubber–road contact: Comparison of physics-based theory and indoor experiments. Tire Sci. Technol. 44, 150–173. https://doi.org/10.2346/tire.16.440303

Mousavi, H., Sandu, C., 2020. Experimental study of the tread rubber compound effects on Tire Performance on Ice. SAE Int. J. Commer. Veh. 13, 99–101. https://doi.org/https://doi.org/10.4271/02-13-02-0006

Mousavi, H., Shenvi, M.N., Sandu, C., 2019. Experimental study for free rolling of tire on ice, in: ASME 2019 International Design Engineering Technical Conferences and Computers and Information in Engineering Conference IDETC/CIE 2019. https://doi.org/10.1115/DETC2019-97846

Nakajima, Y., 2019. Advanced Tire Mechanics, Advanced Tire Mechanics. Springer Nature Singapore, Tokyo, Japan. https://doi.org/10.1007/978-981-13-5799-2

Naranjo, S.D., 2013. Experimental investigation of the tractive performance of an instrumented off road tire on a soft soil terrain. Virginia Polytechnic Institute and State University.

Okel, T.A., Rueby, J.A., 2016. Silica morphology and functionality: Addressing winter tire performance. Rubber World 253, 21–33.

Pacejka, H.B., Bakker, E., 1992. The magic formula tyre model. Veh. Syst. Dyn. 21, 1–18. https://doi.org/10.1080/00423119208969994

Persson, B.N.J., 2006. Rubber friction: Role of the flash temperature. J. Phys. Condens. Matter 18, 7789–7823. https://doi.org/10.1088/0953-8984/18/32/025

Persson, B.N.J., 2011. Rubber friction and tire dynamics. J. Phys. Condens. Matter 23. https://doi.org/10.1088/0953-8984/23/1/015003

Persson, B.N.J., 2014. Role of frictional heating in rubber friction. Tribol. Lett. 56, 77–92. https://doi.org/10.1007/s11249-014-0386-0

Rajamani, R., 2012. Vehicle Dynamics and Control, Integrated Vehicle Dynamics and Control. Springer US. https://doi.org/10.1002/9781118380000.ch5

Ripka, S., Lind, H., Wangenheim, M., Wallaschek, J., Wiese, K., Wies, B., 2012. Investigation of Friction mechanisms of siped tire tread blocks on snowy and icy surfaces. Tire Sci. Technol. 40, 1–24. https://doi.org/10.2346/1.3684409

Sandu, C., Taylor, B., Biggans, J., Ahmadian, M., 2008. Building Infrastructure for Indoor Terramechanics Studies: The Development of a Terramechanics Rig at Virginia Tech, in: Proceedings of 16th ISTVS International Conference, Turin, Italy. Turin, Italy.

Savitski, D., Schleinin, D., Ivanov, V., Augsburg, K., Jimenez, E., He, R., Sandu, C., Barber, P., 2017. Improvement of traction performance and off-road mobility for a vehicle with four individual electric motors: Driving over icy road. J. Terramechanics 69, 33–43. https://doi.org/10.1016/j.jterra.2016.10.005

Skouvaklis, G., Blackford, J.R., Koutsos, V., 2012. Friction of rubber on ice: A new machine, influence of rubber properties and sliding parameters. Tribol. Int. 49, 44–52. https://doi.org/10.1016/j.triboint.2011.12.015

Sokolovskij, E., 2007. Automobile braking and traction characteristics on the different road surfaces. Transport 22, 275–278. https://doi.org/10.1080/16484142.2007.9638141

Tan, T., Xing, C., Tan, Y., 2020. Rubber friction on icy pavement: Experiments and modeling. Cold Reg. Sci. Technol. 174. https://doi.org/10.1016/j.coldregions.2020.103022

US. Department of Transportation, 2020. US DOT: How do weather events impact roads? [WWW Document]. URL https://ops.fhwa.dot.gov/weather/q1_roadimpact.htm (accessed 6.5.20).

US. Department of Transportation, Administration, F.H., 2020. US DOT Road Weather Management Program [WWW Document]. URL https://ops.fhwa.dot.gov/weather/weather_events/snow_ice.htm (accessed 6.5.20).

Van Oosten, J., 1999. TIME, tire measurement procedure: steady state force and moment testing, in: European Automotive Congress.

Weng, P., Tang, Z., Guo, B., 2020. Solving “magic triangle” of tread rubber composites with phosphonium-modified petroleum resin. Polymer (Guildf). 190, 122244. https://doi.org/10.1016/j.polymer.2020.122244

Wiese, K., Kessel, T.M., Mundl, R., Wies, B., 2012. An analytical thermodynamic approach to friction of rubber on ice. Tire Sci. Technol. 40, 124–150.

Xu, F., Yoshimura, K.I., Mizuta, H., 2013. Experimental study on friction properties of rubber material: Influence of surface roughness on sliding friction. Procedia Eng. 68, 19–23. https://doi.org/10.1016/j.proeng.2013.12.141

Yamazaki, S., Yamaguchi, M., Hiroki, E., Suzuki, T., 2000. Effects of the number of siping edges in a tire tread block on Friction Property and Contact with an Icy Road. Tire Sci. Technol. 28, 58–69.

Zhang, Y., Gao, J., Li, Q., 2018. Experimental study on friction coefficients between tire tread rubber and ice. AIP Adv. 8. https://doi.org/10.1063/1.5041049